Annals of Biomedical Engineering (© 2011)
DOI: 10.1007/s10439-011-0482-3

BMES BIOMEDICAL ENGINEERING SOCIETY™ www.bmes.org

Visualizing and Quantifying Acute Inflammation Using ICAM-1 Specific Nanoparticles and MRI Quantitative Susceptibility Mapping

RICHARD WONG,[1,2] XIAOYUE CHEN,[1] YI WANG,[1,2] XUEBO HU,[1] and MOONSOO M. JIN[1,2]

[1]Department of Biomedical Engineering, Cornell University, Ithaca, NY 14853, USA; and [2]Department of Radiology, Weill Cornell Medical College, New York, NY 10022, USA

(*Received 11 August 2011; accepted 28 November 2011*)

Associate Editor Jong Hwan Sung oversaw the review of this article.

Abstract—As intense and prolonged inflammation correlates with the progression of various inflammatory diseases, locating specific regions of the body with dysregulated levels of inflammation could provide crucial information for effective medical diagnosis and treatment. In this study, we demonstrate high resolution spatiotemporal imaging of inflammation in mice treated with systemic injection of lipopolysaccharides (LPS) to mimic systemic inflammatory response or sepsis. Diagnosis of organ-level inflammation was achieved by magnetic resonance imaging (MRI) of inflammation-sensitive superparamagnetic iron oxide (SPIO)-based nanomicelle termed leukocyte-mimetic nanoparticle (LMN), designed to preferentially localize to cells with inflammation-induced overexpression of intercellular adhesion molecule (ICAM)-1. Using a novel MRI quantitative susceptibility mapping (QSM) technique for non-invasive quantification of SPIO nanoparticles, we observed greater accumulation of LMN in the liver, specific to ICAM-1 induction due to LPS-induced inflammation. However, the accumulation of nanoparticles into the spleen appeared to be due to an ICAM-1 independent, phagocytic activity, resulting in higher levels of both LMN and control nanoparticles in the spleen of LPS-treated than untreated mice. Overall, the amounts of nanoparticles in liver and spleen estimated by QSM were in a good agreement with the values directly measured by radioactivity, presenting an idea that spatiotemporal mapping of LMN by MRI QSM may provide a reliable, rapid, non-invasive method for identifying organ-specific inflammation not offered by existing diagnostic techniques.

Keywords—Magnetic resonance imaging, QSM, Sepsis, SPIO, Super paramagnetic iron oxide.

Address correspondence to Moonsoo M. Jin, Department of Radiology, Weill Cornell Medical College, New York, NY 10022, USA. Electronic mail: mj227@cornell.edu

INTRODUCTION

Nonresolving inflammation contributes significantly to the pathogenesis of a variety of human diseases and represents one of the most significant factors of medical burden worldwide.[33] While inflammation is typically initiated in response to harmful stimuli, dysregulation of the inflammation pathways can result in prolonged and excessive inflammation, leading to host damage that can surpass the harm inflicted by the original pathogen.[32] Indeed, unresolving chronic inflammation has been linked to atherosclerosis,[9] obesity,[43] and cancer,[10] prolonged acute inflammation has been closely associated with sepsis[1] and local infections,[34] and the cyclic coexistence of acute and chronic inflammation has been implicated in rheumatoid arthritis,[6] asthma,[4] multiple sclerosis, Crohn's disease, and ulcerative colitis.[33] Of particular concern of inflammatory dysregulation is the intense localized recruitment of macrophages, lymphocytes, and neutrophils to otherwise healthy tissue, resulting in necrosis of vital tissues and organs, contributing greatly to increased patient morbidity and mortality.[11] Thus, identifying localized inflammation in the context of broader inflammation-driven diseases can aid in isolating regions at risk of host-response necrosis and can provide a valuable insight into the progression and severity of the condition.

Current approaches to inflammation detection employ various markers as targets for biospecificity, including soluble extracellular molecules, such as fibrinogen,[29] factor XIII,[21] and collagen,[45] as well as cell surface molecules, such as tissue factor,[24] chondroitin sulfate proteoglycans,[28] vascular adhesion molecule (VCAM-1),[31] and intercellular adhesion molecule (ICAM)-12.[3,30,39] Of particular interest is ICAM-1, a transmembrane molecule that displays

Published online: 06 December 2011

a distinct spatiotemporal response to inflammation. While basally expressed at low levels throughout the body under normal conditions, ICAM-1 is highly inducible under inflammatory stimuli[2] and exhibits highly localized cell surface expression on immune and non-immune cells, such as endothelial cells, fibroblasts, lymphocytes, and myeloid cells.[13] Furthermore, cell surface ICAM-1 overexpression has been linked to various diseases and conditions, and correlates well with inflammation-related tissue and organ damage resulting from hepatic ischemia,[16,17] intestinal and colon ischemias,[36] hepatitis, cirrhosis, Wilson's disease, transplantation rejection,[42] pancreatitis,[44] type 1 diabetes,[12] and multiple organ dysfunction syndrome in sepsis.[1] To target cell surface ICAM-1, we previously employed a high affinity variant of the domain called inserted (I) domain,[22] present in the α subunit of the integrin lymphocyte function-associated antigen (LFA)-1 and solely responsible for LFA-1 interaction with ICAM-1.[27]

One potential application for specific inflammation imaging is for the detection of sepsis. Sepsis is the leading cause of death in critically ill patients admitted to the medical intensive care unit (ICU) in the United States,[3] defined as a systemic inflammatory response to infection manifested by two or more systemic inflammatory response syndrome (SIRS) criteria (such as changes in body temperature, tachycardia, and changes in the number and/or immaturity of white blood cells).[1] Under sepsis, the endothelium experiences sustained and generalized activation, resulting in procoagulant phenotype, increased endothelial cell apoptosis, increased expression of adhesion molecules, and ultimately organ-specific coagulation and dysfunction.[1] As ICAM-1 plays a significant role in mediating leukocyte adhesion as a part of inflammatory response and has been linked to organ-specific inflammation-driven necrosis, identifying sites of high ICAM-1 expression may offer detection or even additional insight into the progression of sepsis or other systemic inflammatory response not offered by existing diagnostic techniques.

In this study, we demonstrate that high resolution spatiotemporal imaging of lipopolysaccharides (LPS)-induced systemic inflammation through the use of inflammation-specific nanoparticles termed leukocyte-mimetic nanoparticles (LMNs),[8] a fluorescently tagged ICAM-1 specific nanomicelle encapsulating superparamagnetic iron oxide (SPIO) nanoparticle as a targeted bimodal near-infrared (IR) optical/magnetic resonance imaging (MRI) contrast agent. Using optical imaging and a novel MRI quantitative susceptibility mapping (QSM) technique,[25] and directly corroborated by radiolabeled isotope measurement, we utilize LMN to quantitatively observe the degree of localized acute inflammation as an indicator of sepsis progression. By tracking the biodistribution of nanoparticles using whole body imaging techniques, we have found greater accumulation of LMN than that of non-ICAM-1 specific controls in the liver of septic mice, while this difference in accumulation was absent in the liver of non-septic mice. In contrast, greater accumulation of nanoparticles irrespective of ICAM-1 targeting was observed in the spleen of septic mice than that of non-septic control, suggesting that localization into the spleen was mainly a result of ICAM-1 independent phagocytic activity. Our study demonstrates the utility of quantitative MRI-based detection of ICAM-1 specific nanoparticles in the major organs including the liver and spleen, organs closely associated with systemic inflammatory response, as a diagnosis method for systemic inflammation through the imaging and quantification of localized inflammation.

MATERIALS AND METHODS

Preparation of ICAM-1 Specific Nanoparticles (Leukocyte-Mimetic Nanoparticles (LMNs))

Details in the synthesis of LMN were described previously.[8] Briefly, oleic acid-capped SPIO nanocrystals (15 nm in diameter, Ocean Nanotech, LLC) were additionally coated with an outer layer of phospholipid, consisting of 1,2-dipalmitoyl-snglycero-3-phosphoethanolamine-*N*-[methoxy(polyethylene glycol)-2000] (DPPE-PEG) and 1,2-dioleoyl-sn-glycero-3-[(*N*-(5-amino-1-carboxypentyl)iminodiacetic acid) succinyl] nickel salt (DOGS-NTA) (Avanti Polar Lipids, Inc.). Radiolabeled lipid-coated SPIO nanoparticles were synthesized by addition of ^{3}H-DPPC (L-α-dipalmitoyl-phosphatidylcholine) (Perkin Elmer) at less than 5% of the total phospholipid to the mixture of DPPE-PEG and DOGS-NTA. The lipid layer on SPIO nanoparticles was formed by hydration of the mixture of lipid-film and SPIO, and lipid-coated SPIO were then purified by density centrifugation, followed by a gel filtration technique. LFA-1 I domains containing mutations of Asp137 $\rightarrow$ Ala (D137A; non-ICAM-1 specific) and Phe265 $\rightarrow$ Ser/Phe292 $\rightarrow$ Gly (F265S/F292G; ICAM-1 specific) fused to His tag (6 histidine residues) at the N-terminal were produced as previously described.[8] Conjugation of lipid-SPIO with His-tagged I domains was obtained by incubation of nanoparticles with I domains at 4 °C overnight, forming LMN (with F265S/F292G) and non-targeting nanoparticle (NTN) (with D137A). All fluorescently labeled nanoparticles were prepared by covalently conjugating Alexa Fluor 750 (AF750) (succinimidyl esters (Invitrogen) to the I domains.

Animal Model of Acute Inflammation

All animal experiments were conducted in compliance with the regulations defined by the Institutional Laboratory Animal Use and Care Committee of Cornell University. 1 mg/mL LPS in 100 μL PBS were injected intravenously through retro-orbital vein into 8-week-old female BALB/c mice 12 h before nanoparticle administration. Prior to imaging hair was removed to reduce background fluorescence. Mice with no treatment were used as negative control. Three mice per group were used for each treatment and imaging regimen.

Near-IR Optical and MR Imaging of Mice

Animals were anesthetized with isoflurane mixed with oxygen at 5% and maintained at 2% isoflurane during whole body imaging (Olympus, OV100). After 12 h treatment with LPS or no-treatment control, mice were administered with 100 μg of nanoparticles coated with AF750-conjugated I domains in 150 μL pH 7.4 PBS *via* retro-orbital injection. Near-IR images of the same mice were taken three times at 1, 8, and 25 h after nanoparticle injection. Image analysis was performed with Matlab R2007a (MathWorks). Mice were euthanized at 1, 8, or 25 h after injection of nanoparticles for MRI by intraperitoneal injection of 2.5% tribromoethanol (20 μL/g), transcardially perfused with pH 7.4 PBS, and fixed in 4% paraformaldehyde. Prepared mice were scanned on a 3T scanner (GE Signa Excite) with 3D multi-echo enhanced fast gradient echo (EFGRE) sequence. Imaging parameters were as follows: TEs 3.696, 4.196, 5.696, 11.696, and 35.696 ms; TR 40 ms; flip angle 30°; matrix size 256 × 64 × 64; voxel size 500 μm isotropic. A 3D Fourier transform was applied to the raw k-space data to reconstruct the images. QSMs were reconstructed using the COSMOS technique, as previously described.[8] Regions of interest were segmented for the liver, spleen, and kidneys, and SPIO localization was estimated using QSM, normalized to a calibration standard.

Histological Sections

At 1 h post-nanoparticle injections, mice were euthanized and perfused with PBS transcardially. Liver tissues were then collected from animals. Part of the tissues were fixed in 4% paraformaldehyde, embedded in paraffin, sliced into 4 μm slides, and stained with hematoxylin and eosin (H&E) or with Perl's Prussian blue. The rest of the tissues were frozen in OCT compounds (Sakura Finetek), sectioned to 10 μm slides, and immunostained with rat anti-mouse CD68 (BioLegend) for detection of macrophages.

Quantification of Radiolabeled LMN

Animals were anesthetized with isoflurane and each was administered with 100 μg ^{3}H-labeled SPIO (600 nCi per mouse) in 100 μL PBS *via* retro-orbital injection. At 1 h post-injection, blood samples were first collected and mice were perfused with PBS and euthanized. Major organs were harvested, homogenized, lysed in tissue solubilizer (Fisher), and then mixed with scintillation counter fluid for radioactivity measurement (Beckman Coulter). Percent distribution into the major organs was obtained after normalization to the total counts of radioisotope decay per animal.

Surface Plasmon Resonance (SPR) Analysis

The affinity of human LFA-1 I domains, F265S/F292G and D137A, to murine ICAM-1 was determined by SPR using BIAcore (BIA2000), as previously described.[22] In brief, a CM5 sensor chip was prepared using an amine coupling kit (BIAcore) to immobilize recombinant murine ICAM-1 fusion with human IgG1 Fc (R & D Systems). Then F265S/F292G and D137A were injected over the chip in injection buffer (20 mM Tris HCl, pH 8.0, 150 mM NaCl, 10 mM $MgCl_2$) at a flow rate of 10 μL/min at RT. In order to examine the specificity of nanoparticle to the level of ICAM-1 expression, CM5 sensor chip was immobilized with three different concentrations of ICAM-1, representing basal to highly induced cell surface density (200, 1000, and 3250 mol/μm^2).[15] Nanoparticles were then flowed over the chip at a flow rate of 15 μL/min to approximate the shear force on nanoparticles *in vivo*.[19]

Statistical Analysis

Statistical analysis was performed using two-way analysis of variance and one-way analysis of variance with Tukey's HSD *post hoc* test at 95% confidence interval (GraphPad Prism).

RESULTS

Previously, we validated the suitability of I domain as a targeting moiety for selective binding of nanoparticles to ICAM-1 overexpression.[8,23,39] In order to design control nanoparticles, termed non-targeted nanoparticle (NTN), we used the same LFA-1 I domain but containing a mutation of D137A, which abolished a ligand-binding site called a metal-ion adhesion site (MIDAS) and subsequently its binding to ICAM-1 (Fig. 1a). SPR measurement confirmed our previous observation with cell staining[8] that human I

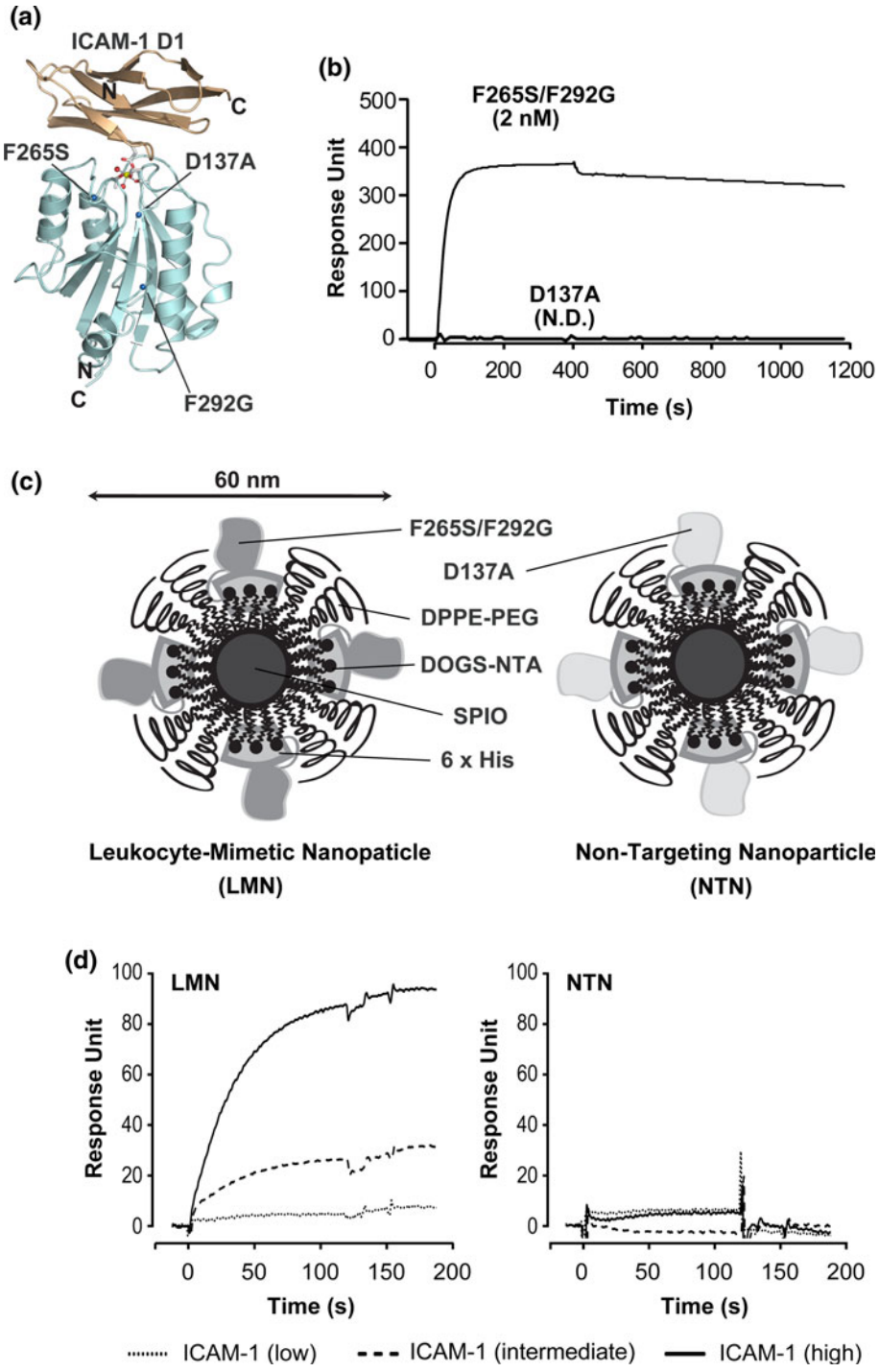

FIGURE 1. Construction of ICAM-1 specific leukocyte-mimetic nanoparticles. (a) Structural model of the complex of ICAM-1 domain 1 and LFA-1 I domain. White spheres depict allosteric activation sites along the peptide backbone. Metal ion and two oxygen atoms of water molecules are depicted as colored spheres. Residues that coordinate to the metal ion are shown as sticks. Mutations of Phe265 → Ser (F265S), Phe292 → Gly (F292G), and Asp137 → Ala (D137A), and N and C termini are indicated. Figure adapted from Fig. 5 of Hu *et al.*[20] (b) SPR measurement of the binding kinetics of I domain variants F265S/F292G and D137A to immobilized murine ICAM-1. F265S/F292G exhibits high ICAM-1 binding affinity (K_D = 2 nM), while variant D137A indicates no (not determinable) binding affinity. (c) Schematic diagram of LMN and NTN. LMN (ICAM-1 specific) and NTN (non-ICAM-1 specific) differ only in surface-conjugated targeting moiety. (d) SPR measurement of the binding kinetics of LMN and NTN to varying concentrations of immobilized ICAM-1 (low, intermediate, and high correspond to approximately 200, 1000, and 3250 mol/μm^2, respectively). LMN binding was limited to the surface coating with higher than normal ICAM-1 site density, while LMN binding to the basal ICAM-1 surface was the same as the background levels seen with NTN.

domain cross-reacted with murine ICAM-1 with comparable affinity to human ICAM-1 ($K_D = 2$ nM to murine ICAM-1 vs. 6 nM to human ICAM-1[22]; Fig. 1b). Subsequent conjugation of F265S/F292G and D137A to prepared lipid-coated SPIO nanoparticles produced LMN and NTN, respectively, through spontaneous assembly from binding of His tag (6× histidine residues) to Nickel-NTA (Fig. 1c).

Prior studies demonstrated that the number of targeting moieties on nanoparticles affected selectivity and targeting efficiency of nanoparticles in binding to cells.[8,18] In order to preferentially target ICAM-1 induced under inflammation but not basally expressed ICAM-1, an optimal ratio of I domain to nanoparticle was empirically determined (~100 molecules per nanoparticle[23]). When an SPR chip was prepared with varying ICAM-1 densities representing basal to high levels of ICAM-1 expression (200, 1000, and 3250 mol/μm^3), LMN binding was limited to the surface coating with higher than normal ICAM-1 site density, while LMN binding to the basal ICAM-1 surface was the same as the background levels seen with NTN (Fig. 1d).

To obtain qualitative assessment of nanoparticle biodistribution, we first imaged each mouse using near-IR optical fluorescence camera. Near-IR optical temporal mapping of the nanoparticle distribution demonstrated greater localization of LMN into the liver in mice treated with LPS (Figs. 2a, 3a). Control nanoparticles (NTN) also exhibited slightly higher accumulation into the liver of LPS-treated mice, which might be attributed to increased ICAM-1 independent phagocytic activity of immune cells or increased blood pool retention due to the inflammation in the liver. Higher fluorescence in the bladder was found to be due to some degree of shedding of the I domains from the nanoparticles, which would be small enough to pass through glomerular capillaries in the kidney and collected into the bladder. After optical imaging, mice were euthanized, transcardially perfused with PBS to remove nanoparticles in the blood, and subjected to MRI to quantitatively map nanoparticle distribution by QSM. Full body temporal mapping of the SPIO distribution was conducted and individual organs were segmented for analysis (Figs. 2b, 2c; S1A, S1B). Specific SPIO quantification of each organ revealed a greater localization of LMN in the liver compared to that of NTN in mice with LPS treatments (Figs. 2b; S1A), peaking at 1 h and progressively diminishing at each subsequent time point. In contrast to higher accumulation of NTN by optical imaging in the liver of LPS-treated mice (Fig. 2a), QSM quantification (Figs. 2b, 3b; S1A, S1B) and radioisotope measurement (Fig. 3c) performed after perfusion revealed that NTN accumulation in the liver was not augmented by LPS treatment, indicating that the higher fluorescence with LPS treatment is due to the increase in the blood pool retention of NTN. While the presence of LPS or the type of nanoparticles administered each independently influenced the magnitude of observable nanoparticle accumulation in the liver, the simultaneous interaction of LMN and LPS had a statistically

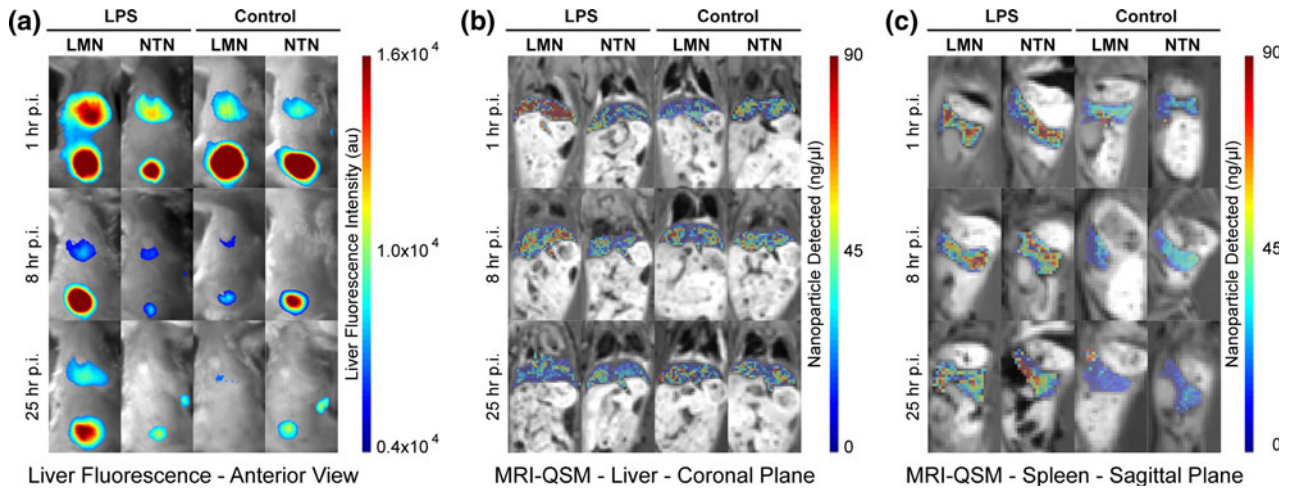

FIGURE 2. Representative images for each treatment regimen obtained using near-IR optical imaging and MRI QSM. (a) Fluorescent heat maps (color) are superimposed over brightfield images (gray scale), indicating greater nanoparticle localization in the liver in LPS/LMN-treated mice compared to that of negative controls, with observable localization diminishing over time. (b–c) MRI QSM reconstructions of the (b) liver and (c) spleen. QSM technique reveals greater nanoparticle localization in the liver of LMN/LPS-treated mice compared to that of negative controls, while greater nanoparticle localization is observed in the spleen in LPS-treated mice, regardless of injected nanoparticle. Portions of these results were previously described in Chen *et al.*,[8] and reproduced here. Representative QSM maps at each time point post-injection (p.i.) of nanoparticles are shown: organ-specific QSM heat maps (color) are superimposed over MRI T2* weighted EFGRE scans used for navigational reference (gray).

significant effect in all measured time points (Table 1). In the spleen, higher amounts of nanoparticle accumulation were detected for LPS-treated mice vs. untreated controls, regardless of the type of nanoparticles used (Figs. 2c, 3b; S1B). Therefore, LPS treatment was the predominant differentiating factor in observable nanoparticle accumulation in the spleen, independent of the targeting moiety or the interaction between LPS treatment and type of nanoparticle injected (Table 1). Negligible amounts of SPIO were detected in the kidneys, supporting the speculation that nanoparticles of ~60 nm in size[8] would be too large for renal filtration.

To further validate MRI quantification of nanoparticles, the values obtained with QSM technique were directly compared to those quantified by measuring radioisotope decay of ^{3}H-labeled nanoparticles. Mice were treated with LPS for 12 h and subsequently injected with ^{3}H-labeled LMN or NTN. At 1 h post-nanoparticle injection, blood was collected and after perfusion and sacrifice of the mice, organs were harvested. Radioactivities of the blood and major organs such as liver, kidney, and spleen were measured and normalized to the total radioactivity of each mouse in order to quantify percent nanoparticle biodistribution in the major organs (Fig. 3c). Highest radioactivity, irrespective of LMN vs. NTN and LPS vs. no treatment, was observed in the blood with a mean radioactivity of ~40%, followed by the levels in the liver

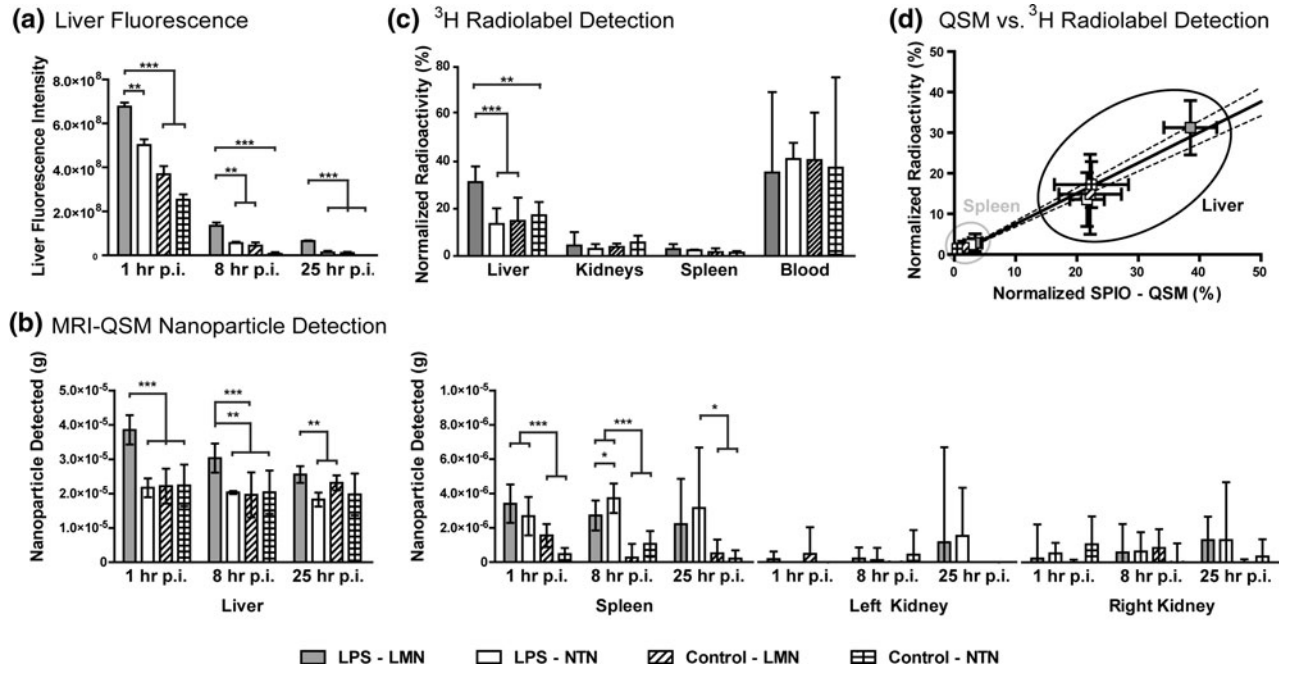

FIGURE 3. Multi-modal quantification of organ-specific nanoparticle localization. (a) Fluorescence detected in the liver region of mice analyzed using near-IR optical imaging at 1, 8, and 25 h post-nanoparticle injection. (b) Measurement of nanoparticle accumulation in the liver, spleen, and kidneys from MRI QSM analysis. (c) Radioactivity measurement of ^{3}H labeled nanoparticles from the liver, kidney, spleen, and blood 1 h post-nanoparticle injection, normalized to the total counts of radioisotope decay per mouse. All modalities measured high liver-specific nanoparticle localization in LPS/LMN-treated mice 1 h post-nanoparticle injection over controls. QSM measured high spleen-specific nanoparticle localization in LPS-treated mice, regardless of nanoparticle injected. Trends persist through 25 h post-nanoparticle injection. Portions of these results were previously described in Chen *et al.*,[8] and reproduced here. One-way analysis of variance with Tukey HSD post-test at 95% confidence interval are summarized in each figure (*$p < 0.001$, **$0.001 < p < 0.01$, *$0.01 < p < 0.05$). (d) Measurements of nanoparticles in the spleen and liver obtained from by radioisotope measurement and by QSM are linearly related. Error bars indicate 95% confidence interval. Dotted line indicates 95% confidence interval for linear regression fitting. $n = 3$ for each treatment and imaging regimen.**

TABLE 1. Two-way analysis of variance of organ-specific nanoparticle accumulation resulting from the treatment of LPS, the type of nanoparticle administered, or due to the interaction between both factors, quantified by QSM technique.

	Liver			Spleen			Right kidney			Left kidney		
Factors	1 h	8 h	25 h	1 h	8 h	25 h	1 h	8 h	25 h	1 h	8 h	25 h
LPS	***	**	ns	***	***	**	ns	ns	*	ns	ns	*
Nanoparticle	***	**	***	**	**	ns	ns	ns	ns	*	*	ns
Interaction	***	**	*	ns	ns	ns	ns	ns	ns	ns	*	ns

***$p < 0.001$; **$0.001 < p < 0.01$; *$0.01 < p < 0.05$; ns no significance.

with significantly higher radioactivity detected in LPS/LMN-treated mice (31.3 ± 6.7%) than those in non-LPS/LMN-treated (14.8 ± 9.9%), LPS/NTN-treated (13.6 ± 6.6%), or non-LPS/NTN-treated controls (17.2 ± 5.7%). Significantly lower amounts (less than 10% of the total) were detected in the lung, kidney, and spleen (Fig. 3c and not shown). Consistent with the QSM measurement of nanoparticle distribution in the spleen, slightly higher amounts of radioactivity were observed in the spleen of LPS-treated (2.7 ± 0.7%) than non-treated (1.5 ± 0.5%) mice. Values obtained by radioisotope measurement and by QSM showed overall an excellent linear relationship ($s_{y.x}$ = 1.60%), with QSM overestimating radioisotope measurements by approximately 25% (Fig. 3d).

In order to examine cellular basis for the increase in LMN accumulation into the liver in LPS-treated mice, selected liver tissues were stained for identification of different types of cells (hepatocyte, endothelium, and Kupffer cells) and localization of nanoparticles (Fig. 4). Vasculature dilatation was apparent in LPS-treated liver tissue (Fig. 4a) with LMN deposited primarily on endothelial cells and Kupffer cells (Fig. 4b). Simultaneous detection of Kupffer cells (CD68) and nanoparticles by Prussian Blue staining revealed that most large deposits of LMN were accumulated into Kupffer cells, implying that higher accumulation of LMN over NTN in the liver of LPS-treated mice is mainly due to ICAM-1 induction and uptake by Kupffer cells.

DISCUSSION

With developments in quantitative MRI techniques, this study presents a clinically adaptable method for

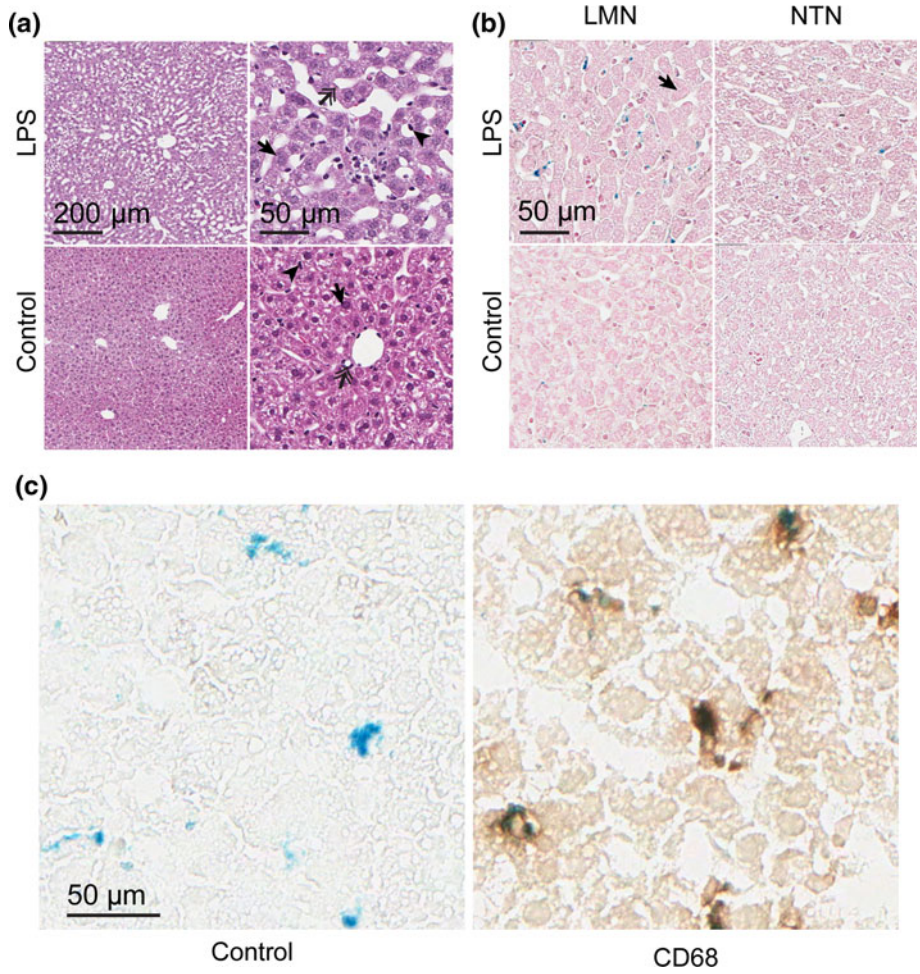

FIGURE 4. Histological sections of liver tissue. (a) H&E stain of liver tissue sections show distinct dilation of liver tissue, characteristic of sepsis. (b) Prussian Blue staining of liver tissue sections shows SPIO accumulation primarily in the endothelial cells and Kupffer cells, with markedly more staining in LPS-treated subjects with injected LMN. (c) CD68 (brown) and Prussian Blue (blue) staining indicates primary localization of iron deposition in Kupffer cells. Examples of hepatocytes (arrow), endothelium (double-headed arrow), and Kupffer cells (arrowhead) are marked.

organ-level mapping of inflammation by quantifying the susceptibility of SPIO-based contrast agents, a measure directly proportional to SPIO concentration. While existing methods for detecting inflammation exist in the context of sepsis diagnosis, such detection methods typically rely on bulk measurements of the presence of pathogens, blood-borne cytokines, and other inflammatory markers, lacking in the spatio-temporal progression and detection of inflammation locally in the body. Central to inflammation is the adhesion of leukocytes to vascular endothelium, a process mediated by molecular interactions between cell adhesion molecules such as integrins and ICAM-1. Toward a sensitive molecular imaging of inflammation, we designed nanoparticles to mimic the ability of leukocyte to preferentially adhere to inflamed vasculature, which was achieved by attaching the high affinity I domain of LFA-1 to nanoparticles. Despite the fact that ICAM-1 is basally expressed in many different types of cells including endothelium and immune cells, our nanoparticles were shown to be selective to vasculature under inflammation with upregulated ICAM-1 expression.[8] Capable of *in vivo* detection by optical imaging and MRI techniques, LMN has previously been shown to specifically localize to the areas of acutely induced local inflammation and to the vasculature within and in the vicinity of the tumor growth, providing spatial and temporal insight into various inflammation-related diseases and conditions. In this study, we demonstrated the potential use of LMN as a bimodal diagnostic agent for the early detection of sepsis or systemic inflammatory response using quantitative MRI techniques.

Previously, we have described a tunable approach to creating nanoparticles that mimic an intrinsic behavior of leukocytes that bind selectively to inflammatory sites.[23] By modulating the affinity and avidity of surface-bound I domains for targeting inflammation, we were able to construct nanoparticles that can resist thermal diffusion and detachment forces exerted by fluid-induced shear stress, while allowing little binding to cells with only basal levels of ICAM-1 expression. Approximately 100 I domains were conjugated to the surface of each LMN, roughly comparable to that of a surface density-optimized approach to ICAM-1 specific nanoparticle design.[18,23] While prior approaches have demonstrated the appeal of employing both selectin ligands and anti-ICAM-1 antibodies to more accurately mimic the rolling and adhesion characteristics of leukocytes,[14,37] we chose to utilize as the targeting moiety for LMN the I domain of LFA-1 integrin, which has been engineered to engage with ICAM-1 with high affinity without prior dependence on interaction with selectins. We found that a targeting moiety derived from physiological molecules, optimized for affinity and avidity, gave superior selectivity and targeting efficiency to inflamed cells in *in vitro* and *in vivo* settings.[8,23]

In treating mice with ICAM-1 specific LMN, we were able to readily differentiate between mice, either pre-treated with LPS or left untreated, by quantitatively measuring nanoparticle localization in various abdominal organs in each of the subjects. This differential effect is most apparent when measuring nanoparticle localization in the liver; a temporal mapping of nanoparticle distribution through MRI QSM demonstrated significantly greater localization of LMN into the liver of sepsis-induced mice compared to that of non-septic subjects, or of those treated with ICAM-1 independent NTN. The observed differences by QSM, corroborated qualitatively by near-IR optometry, were most pronounced 1 h after the treatment of nanoparticles, gradually decaying over time while persisting through at least 24 h after nanoparticle injection. While particles of ~100 nm in diameter in systemic circulation may accumulate in the liver regardless of targeting moiety due to phagocytic activity of immune cells within the liver, the ICAM-1 specificity conferred by the surface conjugation of high affinity I domain (F265S/F292G) of LFA-1 on LMN led to a close to a 2-fold increase in the accumulation in the liver to enable quantitative differentiation. NTN nanoparticles, conjugated with the same LFA-1 I domain but with an inactivating mutation, D137A, did not exhibit higher accumulation into the inflamed liver. This observation was corroborated through histology using iron stating of tissue sections of the liver, revealing a greater degree of nanoparticle accumulation in LPS-treated LMN cases with specific staining observed in both endothelial cells and Kupffer cells with the most significant nanoparticle accumulations co-localized in the Kupffer cells. Thus, while ICAM-1 is basally expressed in all endothelium and utilizing it as a molecular target for inflammation and sepsis imaging techniques may lead to a background signal, it was found that this background binding was negligible, judging from no difference between LMN and NTN accumulations into the liver by radioactivity measurement and QSM. The relationship between LMN biodistribution independent of ICAM-1 expression can be further characterized through the use of ICAM-1 knockout mice or through the use of blocking antibodies to systemically eliminate available ICAM-1 binding sites.

A high degree of nanoparticle localization was also observed in the spleen of LPS-treated mice through optical imaging and QSM. However, unlike the observations in the liver, increases in nanoparticle accumulations to the spleen were observed in all

LPS-treated subjects, regardless of the targeting moiety employed, suggesting that localization is a result of phagocytic activity rather than ICAM-1 biospecificity. Severe and pervasive inflammation, such as that prompted by LPS-induced systemic endotoxic shock, may result in increased phagocytic uptake of nanoparticles in areas in the immediate proximity of major monocyte sources in the spleen, an organ that functions as a major reservoir for undifferentiated monocytes before inflammation-initiated recruitment,[40] and is responsible for the release of splenic lymphokines necessary for the increase of phagocytic activity of macrophages cells in response to inflammatory stimuli.[5,35,41] While studies have indicated high ICAM-1 expression in the epithelial cells of the lungs due to endotoxin-induced inflammation,[7,38] MRI-based techniques such as QSM cannot quantitatively differentiate between signal voids resulting from SPIO-based spin dephasing and signal voids created by air. This difficulty with reliably differentiating QSM-based quantification of SPIO deposits and air may be overcome by multiple data acquisition at differing magnetic field strengths.[26]

Using radiolabeled SPIO nanoparticles, we were able to provide a quantitative mapping of nanoparticle distribution by the measurement of radioactivity and at the same time clinically relevant QSM technique based on MRI. At 1 h post-nanoparticle injection, QSM determined that ~39% of injected nanoparticles were localized into the liver of LPS/LMN mice, a value 70% greater than that of negative controls. In comparison, radioisotope quantification found ~31% of the total body radioactivity was located in the liver of LPS/LMN-treated mice, a value 81% greater than that of negative controls. However, some difference in QSM quantification vs. radioactivity measurement of nanoparticles was unavoidable as it was found that the lipid layer outside of SPIO was subject to some degree of shedding during circulation. This may explain, in the course of optical imaging, varying degrees of fluorescence (conjugated to the I domains) observed in the bladder of each subject, regardless of the nanoparticle targeting moiety. The decoupling of the fluorescence or protein from nanoparticles was found to be caused by shedding of the phospholipid lipid layer from SPIO or lipid degradation by phospholipase activity in the plasma, but not due to dissociation between His tag and Ni–NTA, judging from a dramatic decrease in decoupling when crosslinkable fatty acids were used to cage SPIO (data not shown).

Sepsis represents a continuum in clinical-pathologic severity with definable phases that characterize patients at risk for increased mortality. Current diagnosis techniques have limited windows of detection and may rely on transient biology and physiological conditions that may not persist across all phases of sepsis progression. Moreover, the onset of sepsis can be linked to a widely heterogeneous set of initial risk factors, further complicating diagnosis and delaying treatment. In particular, the endothelium is crucial in regulating a local balance between pro-inflammatory and anti-inflammatory mediators; under sepsis, endothelium undergoes excessive, sustained, and generalized activation, resulting in unregulated expression of inflammation-associated products. Among these, adhesion molecule ICAM-1 has been implicated as a highly localized biomarker for inflammation induced under organ damage,[17,36,42] one of the most significant mortality risks in septic patients.[1] By specifically targeting ICAM-1 using bimodal LMN, we were able to readily differentiate septic and non-septic mice using optical imaging and quantitative MRI techniques, both non-invasive modalities. Most significantly, the observed differences were pronounced as soon as 1 h after the treatment of the nanoparticle, and persist through at least 25 h after injection. In this study, our temporal mapping of inflammation was focused on following nanoparticle distribution over 25 h in mice exposed to LPS for 12 h. However, as surface-expressed ICAM-1 is induced rapidly under inflammation, with some studies observing peak expression as quickly as 1–2 h after the introduction of stimuli,[2] additional information on spatiotemporal dynamics of inflammation can be obtained by subjecting mice to different durations of LPS while maintaining similar post-treatment imaging protocols. Such information on spatiotemporal dynamics of inflammation would be necessary to better understand the distinct yet common processes of inflammation in reticuloendothelial systems such as the liver and spleen.

This study also reveals the strength of MRI QSM in quantitatively measuring contrast agent localization into specific structures within the body. While optical imaging provides a gross view of the overall biodistribution of a fluorescent marker, the results are coarse, qualitative in nature, and prone to confounding effects due to the relatively shallow penetration depth of common fluorescent wavelengths, and the technique is not ideal for most clinical applications. Alternatively, traditional MRI techniques, such as typical T2* weighted imaging, provide significantly greater spatial resolution, but visualization is hindered by large obscuring signal voids resulting from SPIO use, and the resulting images are largely qualitative in nature, making it difficult to precisely estimate SPIO localization. In contrast, QSM technique offers a quantitative, high resolution method of tracking the biodistribution of paramagnetic contrast agents to specific organs and structures through mapping of magnetic susceptibility, a physical property of paramagnetic materials that relates linearly to its

concentration, allowing for direct determination of the amount and spatial location of contrast agent accumulation. Moreover, while SPIO-based contrast agents may result in signal voids in traditional T2* imaging and obscured underlying structure, QSM reconstruction techniques enable unimpeded analysis of the distribution of contrast agent and spatiotemporal mapping of inflammation. Given the speed and robustness by which these differences can be observed after administration of LMN, this technique offers temporal flexibility ideal for clinical applications, while granting dramatically increased spatial fidelity not offered by existing bulk measurement diagnostic techniques.

ELECTRONIC SUPPLEMENTARY MATERIAL

The online version of this article (doi:10.1007/s10439-011-0482-3) contains supplementary material, which is available to authorized users.

ACKNOWLEDGMENTS

Support for this work was provided in part by NSF GK-12 Fellowship and American Heart Association Scientist Development Grant (M.M.J.).

CONFLICT OF INTEREST

No benefits in any form have been or will be received from a commercial party related directly or indirectly to the subject of this manuscript.

REFERENCES

[1]Aird, W. C. The role of the endothelium in severe sepsis and multiple organ dysfunction syndrome. *Blood* 101(10): 3765–3777, 2003.

[2]Almenar-Queralt, A., A. Duperray, L. A. Miles, J. Felez, and D. C. Altieri. Apical topography and modulation of ICAM-1 expression on activated endothelium. *Am. J. Pathol.* 147(5):1278–1288, 1995.

[3]Angus, D. C., W. T. Linde-Zwirble, J. Lidicker, G. Clermont, J. Carcillo, and M. R. Pinsky. Epidemiology of severe sepsis in the United States: analysis of incidence, outcome, and associated costs of care. *Crit. Care Med.* 29(7):1303–1310, 2001.

[4]Barnes, P. J. Immunology of asthma and chronic obstructive pulmonary disease. *Nat. Rev. Immunol.* 8(3): 183–192, 2008.

[5]Billiar, T. R., M. A. West, B. J. Hyland, and R. L. Simmons. Splenectomy alters Kupffer cell response to endotoxin. *Arch. Surg.* 123(3):327–332, 1988.

[6]Buckley, C. D., D. Pilling, J. M. Lord, A. N. Akbar, D. Scheel-Toellner, and M. Salmon. Fibroblasts regulate the switch from acute resolving to chronic persistent inflammation. *Trends Immunol.* 22(4):199–204, 2001.

[7]Burns, A. R., F. Takei, and C. M. Doerschuk. Quantitation of ICAM-1 expression in mouse lung during pneumonia. *J. Immunol.* 153(7):3189–3198, 1994.

[8]Chen, X., R. Wong, I. Khalidov, A. Y. Wang, J. Leelawattanachai, Y. Wang, and M. M. Jin. Inflamed leukocyte-mimetic nanoparticles for molecule imaging of inflammation. *Biomaterials* 32(30):7651–7661, 2011.

[9]Corti, R., R. Hutter, J. J. Badimon, and V. Fuster. Evolving concepts in the triad of atherosclerosis, inflammation and thrombosis. *J. Thromb. Thrombolysis* 17(1):35–44, 2004.

[10]Coussens, L. M., and Z. Werb. Inflammation and cancer. *Nature* 420(6917):860–867, 2002.

[11]Deitch, E. A. Multiple organ failure. Pathophysiology and potential future therapy. *Ann. Surg.* 216(2):117–134, 1992.

[12]Denis, M. C., U. Mahmood, C. Benoist, D. Mathis, and R. Weissleder. Imaging inflammation of the pancreatic islets in type 1 diabetes. *Proc. Natl. Acad. Sci. USA* 101(34): 12634–12639, 2004.

[13]Dustin, M. L., R. Rothlein, A. K. Bhan, C. A. Dinarello, and T. A. Springer. Induction by IL 1 and interferon-gamma: tissue distribution, biochemistry, and function of a natural adherence molecule (ICAM-1). *J. Immunol.* 137(1): 245–254, 1986.

[14]Eniola, A. O., and D. A. Hammer. Characterization of biodegradable drug delivery vehicles with the adhesive properties of leukocytes II: effect of degradation on targeting activity. *Biomaterials* 26(6):661–670, 2005.

[15]Eniola, A. O., P. J. Willcox, and D. A. Hammer. Interplay between rolling and firm adhesion elucidated with a cell-free system engineered with two distinct receptor-ligand pairs. *Biophys. J.* 85(4):2720–2731, 2003.

[16]Essani, N. A., M. A. Fisher, A. Farhood, A. M. Manning, C. W. Smith, and H. Jaeschke. Cytokine-induced upregulation of hepatic intercellular adhesion molecule-1 messenger RNA expression and its role in the pathophysiology of murine endotoxin shock and acute liver failure. *Hepatology* 21(6):1632–1639, 1995.

[17]Farhood, A., G. M. McGuire, A. M. Manning, M. Miyasaka, C. W. Smith, and H. Jaeschke. Intercellular adhesion molecule 1 (ICAM-1) expression and its role in neutrophil-induced ischemia-reperfusion injury in rat liver. *J. Leukoc. Biol.* 57(3):368–374, 1995.

[18]Haun, J. B., and D. A. Hammer. Quantifying nanoparticle adhesion mediated by specific molecular interactions. *Langmuir* 24(16):8821–8832, 2008.

[19]Holme, P. A., U. Orvim, M. J. Hamers, N. O. Solum, F. R. Brosstad, R. M. Barstad, and K. S. Sakariassen. Shear-induced platelet activation and platelet microparticle formation at blood flow conditions as in arteries with a severe stenosis. *Arterioscler. Thromb. Vasc. Biol.* 17(4):646–653, 1997.

[20]Hu, X., S. Kang, X. Chen, C. B. Shoemaker, and M. M. Jin. Yeast surface two-hybrid for quantitative in vivo detection of protein–protein interactions via the secretory pathway. *J. Biol. Chem.* 284(24):16369–16376, 2009.

[21]Jaffer, F. A., C. H. Tung, J. J. Wykrzykowska, N. H. Ho, A. K. Houng, G. L. Reed, and R. Weissleder. Molecular imaging of factor XIIIa activity in thrombosis using a novel, near-infrared fluorescent contrast agent that covalently links to thrombi. *Circulation* 110(2):170–176, 2004.

[22]Jin, M., G. Song, C. V. Carman, Y. S. Kim, N. S. Astrof, M. Shimaoka, D. K. Wittrup, and T. A. Springer. Directed

evolution to probe protein allostery and integrin I domains of 200,000-fold higher affinity. *Proc. Natl. Acad. Sci. USA* 103(15):5758–5763, 2006.
[23]Kang, S., T. Park, X. Chen, G. Dickens, B. Lee, K. Lu, N. Rakhilin, S. Daniel, and M. M. Jin. Tunable physiologic interactions of adhesion molecules for inflamed cell-selective drug delivery. *Biomaterials* 32(13):3487–3498, 2011.
[24]Lanza, G. M., X. Yu, P. M. Winter, D. R. Abendschein, K. K. Karukstis, M. J. Scott, L. K. Chinen, R. W. Fuhrhop, D. E. Scherrer, and S. A. Wickline. Targeted antiproliferative drug delivery to vascular smooth muscle cells with a magnetic resonance imaging nanoparticle contrast agent: implications for rational therapy of restenosis. *Circulation* 106(22):2842–2847, 2002.
[25]Liu, T., P. Spincemaille, L. de Rochefort, B. Kressler, and Y. Wang. Calculation of susceptibility through multiple orientation sampling (COSMOS): a method for conditioning the inverse problem from measured magnetic field map to susceptibility source image in MRI. *Magn. Reson. Med.* 61(1):196–204, 2009.
[26]Liu, T., P. Spincemaille, L. de Rochefort, R. Wong, M. Prince, and Y. Wang. Unambiguous identification of superparamagnetic iron oxide particles through quantitative susceptibility mapping of the nonlinear response to magnetic fields. *Magn. Reson. Imaging* 28(9):1383–1389, 2010.
[27]Marlin, S. D., and T. A. Springer. Purified intercellular adhesion molecule-1 (ICAM-1) is a ligand for lymphocyte function-associated antigen 1 (LFA-1). *Cell* 51(5):813–819, 1987.
[28]Massey, J. M., J. Amps, M. S. Viapiano, R. T. Matthews, M. R. Wagoner, C. M. Whitaker, W. Alilain, A. L. Yonkof, A. Khalyfa, N. G. Cooper, J. Silver, and S. M. Onifer. Increased chondroitin sulfate proteoglycan expression in denervated brainstem targets following spinal cord injury creates a barrier to axonal regeneration overcome by chondroitinase ABC and neurotrophin-3. *Exp. Neurol.* 209(2):426–445, 2008.
[29]McAteer, M. A., A. M. Akhtar, C. von Zur Muhlen, and R. P. Choudhury. An approach to molecular imaging of atherosclerosis, thrombosis, and vascular inflammation using microparticles of iron oxide. *Atherosclerosis* 209(1):18–27, 2010.
[30]Muro, S., C. Gajewski, M. Koval, and V. R. Muzykantov. ICAM-1 recycling in endothelial cells: a novel pathway for sustained intracellular delivery and prolonged effects of drugs. *Blood* 105(2):650–658, 2005.
[31]Nahrendorf, M., F. A. Jaffer, K. A. Kelly, D. E. Sosnovik, E. Aikawa, P. Libby, and R. Weissleder. Noninvasive vascular cell adhesion molecule-1 imaging identifies inflammatory activation of cells in atherosclerosis. *Circulation* 114(14):1504–1511, 2006.
[32]Nathan, C. Points of control in inflammation. *Nature* 420(6917):846–852, 2002.
[33]Nathan, C., and A. Ding. Nonresolving inflammation. *Cell* 140(6):871–882, 2010.
[34]Nathan, C., and M. Sporn. Cytokines in context. *J. Cell Biol.* 113(5):981–986, 1991.
[35]Nogueira, N., and Z. A. Cohn. Trypanosoma cruzi: in vitro induction of macrophage microbicidal activity. *J. Exp. Med.* 148(1):288–300, 1978.
[36]Olanders, K., Z. Sun, A. Borjesson, M. Dib, E. Andersson, A. Lasson, T. Ohlsson, and R. Andersson. The effect of intestinal ischemia and reperfusion injury on ICAM-1 expression, endothelial barrier function, neutrophil tissue influx, and protease inhibitor levels in rats. *Shock* 18(1):86–92, 2002.
[37]Omolola Eniola, A., and D. A. Hammer. In vitro characterization of leukocyte mimetic for targeting therapeutics to the endothelium using two receptors. *Biomaterials* 26(34):7136–7144, 2005.
[38]Panes, J., M. A. Perry, D. C. Anderson, A. Manning, B. Leone, G. Cepinskas, C. L. Rosenbloom, M. Miyasaka, P. R. Kvietys, and D. N. Granger. Regional differences in constitutive and induced ICAM-1 expression in vivo. *Am J Physiol* 269(6 Pt 2):H1955–H1964, 1995.
[39]Park, S., S. Kang, A. J. Veach, Y. Vedvyas, R. Zarnegar, J. Y. Kim, and M. M. Jin. Self-assembled nanoplatform for targeted delivery of chemotherapy agents via affinity-regulated molecular interactions. *Biomaterials* 31(30):7766–7775, 2010.
[40]Swirski, F. K., M. Nahrendorf, M. Etzrodt, M. Wildgruber, V. Cortez-Retamozo, P. Panizzi, J. L. Figueiredo, R. H. Kohler, A. Chudnovskiy, P. Waterman, E. Aikawa, T. R. Mempel, P. Libby, R. Weissleder, and M. J. Pittet. Identification of splenic reservoir monocytes and their deployment to inflammatory sites. *Science* 325(5940):612–616, 2009.
[41]Van Snick, J. Interleukin-6: an overview. *Annu. Rev. Immunol.* 8:253–278, 1990.
[42]Volpes, R., J. J. van den Oord, and V. J. Desmet. Immunohistochemical study of adhesion molecules in liver inflammation. *Hepatology* 12(1):59–65, 1990.
[43]Wellen, K. E., and G. S. Hotamisligil. Obesity-induced inflammatory changes in adipose tissue. *J. Clin. Invest.* 112(12):1785–1788, 2003.
[44]Werner, J., K. Z'Graggen, C. Fernandez-del Castillo, K. B. Lewandrowski, C. C. Compton, and A. L. Warshaw. Specific therapy for local and systemic complications of acute pancreatitis with monoclonal antibodies against ICAM-1. *Ann. Surg.* 229(6):834–840, 1999, discussion 841–832.
[45]Wilson, M. S., and T. A. Wynn. Pulmonary fibrosis: pathogenesis, etiology and regulation. *Mucosal Immunol.* 2(2):103–121, 2009.